can be estimated as

$$\frac{E_0}{m_e c^2} L_{e^+} ,$$

where E_0 is the initial particle energy. For example, if positrons are produced by cosmic rays (via π^+-meson formation), the minimal expenditure of power equals $\approx 3 \times 273 \times L_{e^+} \approx 10^{40}$ erg s^{-1}. Here, we have taken into account that π^- and π^0 mesons are produced simultaneously with π^+ mesons. Decay of π^0 mesons must give rise to gamma emission at energies of 50 – 100 MeV with a luminosity on the order of 3×10^{39} erg s^{-1}. All these estimates, of course, have been obtained by assuming the stationarity of the annihilation emission.

An analysis of data gathered in the first series of observations indicates that the contribution from the disk component is smaller than the radiant flux from the central part of the Galaxy [6, 7]. The luminosity ratio is a model-dependent quantity strongly depending on the assumed properties of individual components, for example, on the disk component thickness.

The center of the line coincides with the rest energy of electrons (positrons) with high accuracy:

$$\frac{E}{m_e c^2} = 0.99991 \pm 0.00015 .$$

Therefore, the mean line-of-sight velocity of the medium with reference to the Earth is no more than ~ 44 km s^{-1}. Observations of the annihilation linewidth also allow us to impose restrictions on the characteristic velocity of chaotic motions in the medium. The intrinsic linewidth in a medium at rest depends on the temperature and degree of its ionization (see Fig. 4) and can be sufficiently small ($\sim 1 - 1.5$ keV). Taking this into account, a conservative upper bound on the spread in the line-of-sight velocity amounts to ~ 800 km s^{-1}.

The combination of the observed linewidth (2.37 ± 0.25 keV) and positronium fraction ($F_{PS} = 0.96 \pm 0.04$) can be explained by annihilation in a 'warm' phase of the interstellar medium with a characteristic temperature of around 8000 K and degree of its ionization on the order of 0.1. Annihilation in a single-phase cold ($T \leqslant 10^3$ K) or hot ($T \geqslant 10^5$ K) medium is inconsistent with the measurement data. However, a combination comprising several phases with different temperatures and degrees of ionization cannot also be excluded. The limit on the annihilation fraction in a very hot ($T \geqslant 10^6$ K) phase is below 8%.

The characteristics of the annihilation emission given above evidence against models of the positron origin in type II supernovae and massive stars, since such objects are found exclusively in the disk of the Galaxy and not in its bulge. Likewise (and from the energy consideration), a hypothesis for the production of positrons by interactions of cosmic rays with matter seems improbable. The INTEGRAL observatory data are more consistent with positron sources populating the Galactic bulge, in particular, with type Ia supernovae, low-mass binaries, or dark matter annihilation. Each of these mechanisms has its own advantages and shortcomings. One of the most important goals of continuing INTEGRAL observations is to impose more stringent constraints on the surface brightness distribution and spectral shape variations in the annihilation emission along and across the galactic plane. This will allow us to significantly narrow the class of physical processes mainly responsible for the production of positrons in the Galaxy.

References

1. Johnson W N (III), Harnden F R (Jr), Haymes R C *Astrophys. J.* **172** L1 (1972)
2. Leventhal M, MacCallum C J, Stang P D *Astrophys. J.* **225** L11 (1978)
3. Vedrenne G et al. *Astron. Astrophys.* **411** L63 (2003)
4. Churazov E et al. *Mon. Not. R. Astron. Soc.* **357** 1377 (2005)
5. Churazov E et al. *Astrophys. J.* **471** 673 (1996)
6. Teegarden B J et al. *Astrophys. J.* **621** 296 (2005)
7. Knödlseder J et al. *Astron. Astrophys.* **441** 513 (2005)
8. Bussard R W, Ramaty R, Drachman R J *Astrophys. J.* **228** 928 (1979)
9. Kernoghan A A et al. *J. Phys. B: At. Mol. Opt. Phys.* **29** 2089 (1996)
10. Gould R J *Astrophys. J.* **344** 232 (1989)
11. Bhatia A K, Drachman R J, Temkin A *Phys. Rev. A* **16** 1719 (1977)
12. Swartz W E, Nisbet J S, Green A E S *J. Geophys. Res.* **76** 8425 (1971)
13. Iwata K, Greaves R G, Surko C M *Phys. Rev. A* **55** 3586 (1997)
14. McKee C F, Ostriker J P *Astrophys. J.* **218** 148 (1977)
15. Kaplan S A, Pikel'ner S B *Fizika Mezhzvezdnoi Sredy* (Physics of Interstellar Medium) (Moscow: Nauka, 1979)
16. Crannell C J et al. *Astrophys. J.* **210** 582 (1976)
17. Jean P et al. *Astron. Astrophys.* **445** 579 (2006)

PACS numbers: **97.80.–d**, **98.70.–f**, 98.70.Qy
DOI: 10.1070/PU2006v049n03ABEH005970

Ultraluminous X-ray sources in galaxies — microquasars or intermediate mass black holes

S N Fabrika, P K Abolmasov, S V Karpov, O N Sholukhova, K K Ghosh

1. New class of X-ray sources

Ultraluminous X-ray sources (ULXs) in external galaxies were singled out in astrophysics as a new class of objects in 2000. Very bright X-ray sources had been discovered in galaxies earlier [1]. However, only after NASA's CHANDRA X-ray Observatory observations with a spatial resolution of $\approx 1''$ did it become clear that they constitute a new class of objects. These objects are not active galactic nuclei and not background quasars . In our report we briefly describe intriguing properties of these objects, basic models proposed for ULXs, and ideas that could help in understanding the nature of ULXs from analysis by observational methods. The last, in particular, includes studies of gaseous nebulae surrounding these objects, carried out on the 6-meter telescope of the Special Astrophysical Observatory (SAO) of RAS, as well as predictions of the specific X-ray spectra of ULXs.

ULXs are distinguished by their huge X-ray luminosities of $10^{39} - 10^{42}$ egr s^{-1} in the 0.5 – 100 keV energy range. In our Galaxy, the maximum observed luminosities from accreting black holes in close binaries amount to $\sim 10^{38}$ erg s^{-1} in 'persistent' emission (i.e., not at the peak of an outburst). In this case, measured masses of the black holes fall within the range 4 – 15 solar masses. The total X-ray luminosity of a galaxy like our own or M31 ranges $(0.5 - 1) \times 10^{40}$ erg s^{-1} (2 – 20 keV). The critical luminosity of an accreting black

hole, or the Eddington luminosity at which radiation pressure is balanced by gravitational attraction of gas by the black hole, is $\approx 10^{38}$ erg s^{-1} for one solar mass, or $\approx 10^{39}$ erg s^{-1} for the 'typical' black hole mass. This implies that if radiation from ULXs is isotropic, their black hole masses can be as high as 10,000 solar masses.

X-ray emission from ULXs is strongly variable on time scales of a few dozen seconds to several years. No clear periodicities have been found, and yet quasiperiodic oscillations have been discovered [2] on time scales of ~ 20 s. Ultraluminous X-ray sources are distant objects registered in galaxies lying at distances of 3 Mpc and beyond, so searches for rapid brightness variability in ULXs have been restricted thus far by the sensitivity of X-ray observatories. The X-ray spectra of ULXs do not demonstrate pronounced spectral features; X-ray continuum is well fitted in average by a power-law $f_E \propto E^{-\alpha}$ with $\alpha = 0.5 - 2$, or by the so-called 'multicolor disk' (MCD) spectrum, which is defined as the spectrum of integral emission from a standard Shakura – Sunyaev accreting disk [3] with a temperature at the inner disk edge of $T_{\rm in} \sim 1-3$ keV. In this approximation, ULX spectra are quite similar to those of 'classical' stellar mass black holes, but the diversity of ULX spectra is fairly broad.

The principal property of ULXs is their location in star forming regions near galactic nuclei or in spiral arms of spiral or interacting galaxies. Studies on X-ray luminosity functions of galaxies [4] are in their infancy, however, it is already known that the number of X-ray sources in galaxies is proportional to the star formation rate. The frequency of ULXs (the bright end of the luminosity functions) is also determined by the star formation rate. A very crude estimate of the ULX frequency reduces to one object per ~ 20 spiral galaxies [5].

Clearly, ULXs are related to the young stellar population, i.e., to massive stars. Probably for this reason ULXs are frequently (or always) surrounded by gaseous nebulae. The nebulae around these objects have sizes from 10 to several hundred pc. Sometimes ULXs reside in the region of young star clusters. Clusters illuminate nebulae in sizes up to 300 – 400 pc, i.e., in this case large nebulae are genetically related to star clusters in which a ULX object emerged. Young (i.e., massive, bright and hot) stars not brighter than 20 – 22 stellar magnitudes are found within error boxes of these X-ray sources, so that the spectroscopy of these stars is difficult.

Presently, two models for ULXs are under consideration. According to the first model, ULXs represent supercritical accretion disks (SCADs) in binary systems with stellar mass black holes ($\sim 10 M_\odot$), observed close to the disk axis [5, 6]. Black holes in binary systems that produce relativistic jets are called microquasars [7]. In this case, the real luminosity of a ULX can be much smaller: we observe X-ray radiation which is geometrically collimated in a funnel of SCAD and can also be relativistically amplified. The second model suggests that ULXs constitute 'intermediate' black holes, with masses between stellar values and those of supermassive black holes in galactic nuclei (IMBH, $10 - 10{,}000 M_\odot$), surrounded by standard accretion disks [8, 9]. Assuming that a black hole has a large mass we broaden the allowed luminosity range. IMBHs are called missed class of astrophysical objects. In the most successful cosmological scenarios, supermassive stars with masses exceeding 100 solar masses must be formed at redshifts $z = 20-25$ ('the population III'). These stars should have left black holes that after the formation of galaxies were captured in galactic halos. Such black holes can accrete interstellar gas or capture stars in close orbits and are likely to be observed as ULXs [10]. Realistic estimates show that for luminosities as observed in ULXs the accretion rate of gas onto the black hole must be $\sim 10^{-6} M_\odot$ per year. In order for the interstellar gas accretion to proceed, the surrounding conditions for an IMBH must be very specific. For IMBH to capture a donor star, the latter would have to be a massive star. Any of these conditions sharply decreases the frequency of IMBH seen as ULXs.

Here, we argue in favor of the first model for ULXs, especially because such X-ray sources in galaxies were predicted [5] from studies of the galactic object SS 433. This is a unique object in the Galaxy comprising a close binary system with a black hole $\sim 10 M_\odot$ persistently accreting gas with a highly supercritical rate [7, 11, 12]. The evolution stage of the donor in SS 433 (mass loss on the 'thermal time scale') is very short, $10^4 - 10^5$ years, which explains the rarity of such objects. The orientation of the SS 433 system is such that the observer cannot 'look' into the supercritical accretion disk funnel. In paper [5], we discussed observational appearances of SS 433 type objects (more precisely, of SS 433 itself) seen close to the disk and relativistic jet axis and concluded that such objects can form a new class of extragalactic X-ray sources. We continue to develop the idea that ULXs are supercritical accretion disks like SS 433, viewed under favorable orientation. In what follows we shall describe two crucial experiments: (1) observations of nebulae around ULXs and their comparison to the nebula around SS 433; in contrast to stars, extended nebulae turn out to be quite bright at megaparsec distances; analysis of emission lines of the nebulae allows fairly reliable diagnostics of the gas ionization source, and (2) the study of possible properties of the funnel in a supercritical accretion disk, enabling the prediction of the X-ray spectrum of ULXs.

2. Nebulae surrounding ULXs and SS 433

SS 433 is surrounded by an elongated radio nebula W 50 produced by the interaction of SS 433's jets with the ambient interstellar medium [13]. The nebula emits synchrotron radiation and relativistic electrons appear due to a deceleration of jets. At the jet deceleration sites ($\sim \pm 50$ pc from the center), bright optical filaments emitting hydrogen lines and forbidden lines of sulfur, nitrogen, and oxygen are observed. The filamentary structure expands with a velocity of about 50 km s^{-1}. Nebulae around ULXs, studied by us, have similar sizes and luminosities in emission lines, and almost the same total energetics ranging $10^{51} - 10^{52}$ erg [14].

In Figure 1 we present maps of the MF 16 nebula surrounding the ULX in the galaxy NGC 6946 as obtained by observations with the 6-meter telescope BTA SAO RAS. The multipupil field spectrograph (MPFS) [15] with an angular resolution of $1''$ has been used. In the [OIII] lines, a velocity gradient along the nebula in the East – West direction was discovered. More detailed later observations carried out with the SCORPIO spectrograph [17] revealed that the velocity variation along the nebula (its size is around 20 pc) reaches 100 km s^{-1}.

Figure 2 demonstrates the results of observations by the same instrument of the nebula surrounding ULX-1 in the galaxy IC 342. We also detected a velocity gradient (overall expansion of the nebula) equal to ± 20 km s^{-1}. This nebula is fairly dim as the light from the galaxy IC 342 itself is strongly absorbed by dust in the Milky Way.

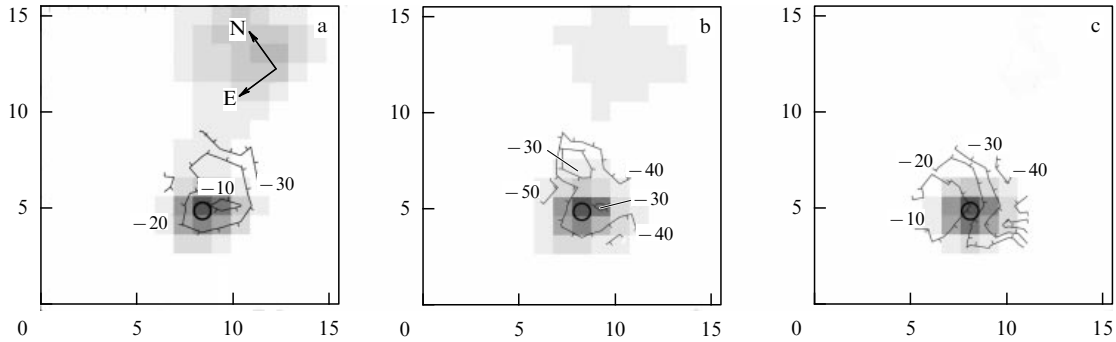

Figure 1. Results of integral-field spectroscopy of the nebula MF 16 surrounding a ULX in the galaxy NGC 6946. Maps of 15″ × 15″ regions in Hα (a), [SII] λ 6717, 6734 (b), and [OIII] λ 4959, 5007 (c) lines are presented. The circle marks the position of the X-ray source as observed by the CHANDRA X-ray Observatory. Lines of equal radial velocities (in units [km s^{-1}]) are shown. The lines' hatches indicate the direction of the radial velocity gradient.

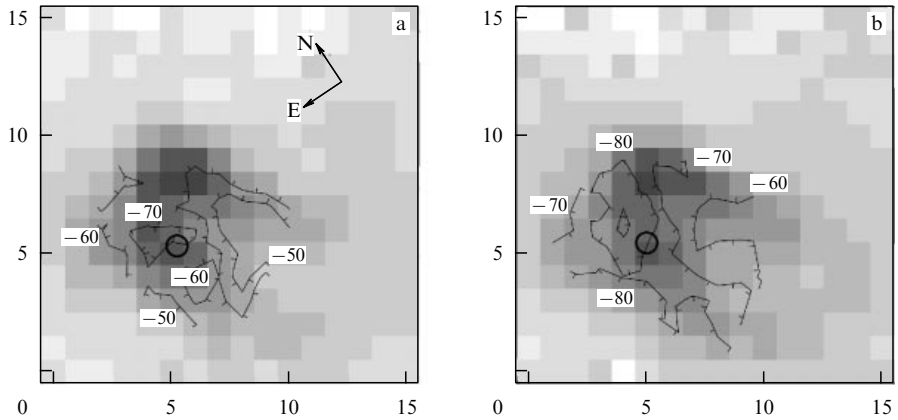

Figure 2. Integral-field spectroscopy of the nebula surrounding ULX-1 in the galaxy IC 342. Maps in Hα (a) and [SiII] λ 6717, 6734 (b) lines are shown. Other notations as in Fig. 1.

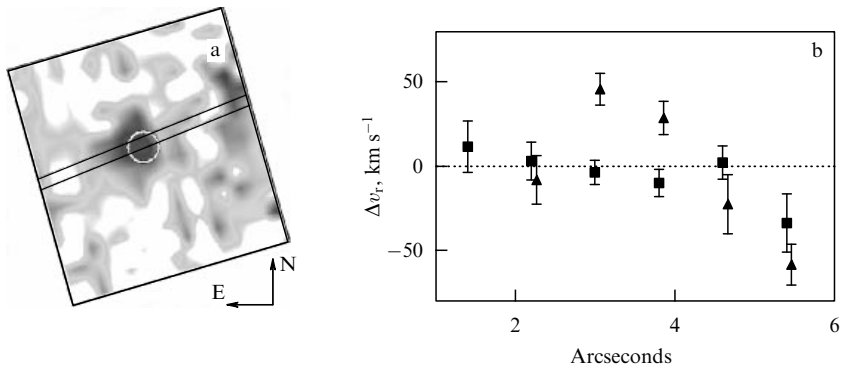

Figure 3. Integral-field spectroscopy of the nebula surrounding a ULX in the Holmberg II galaxy. (a) Map in the HeII λ 4686 line; two straight lines mark the position of the spectrograph slits. (b) The radial velocity difference in this line and in the [OIII] line measured along the nebula [18]; squares and triangles correspond to the upper and lower slit, respectively.

In Fig. 3 we present the results of observations by the same instrument of the nebula surrounding a ULX in the galaxy Holmberg II. A velocity gradient of ±50 km s^{-1} was also discovered on scales of ±50 pc [18]. The velocity along the nebula was measured in more detail by the BTA slit spectrograph.

In all three nebulae we observed, the intensity ratios of the diagnostic lines testify to collisional gas ionization (by shocks). Two additional conclusions directly relating to the physics of the central source are as follows.

(1) The gas velocity gradients of 50 – 100 km s^{-1} on scales of 20 – 100 pc suggest dynamically disturbed nebulae. An IMBH cannot disturb gas on such scales, as the Bondi capture radius is no more than 0.1 pc. In addition, these nebulae are too large and energetic to fit standard relations for supernova remnants. These nebulae are very likely to be powered by the central object via jet activity, as in the case of SS 433 galactic object.

(2) An additional source of hard UV radiation is necessary to explain the luminosity in high-excitation lines and the line spectrum. The luminosity of this source ($\sim 10^{40}$ erg s^{-1}) is as high as the X-ray luminosity.

In Fig. 4, we present images of the three nebulae at the same linear scale. Ring-like structures are visible on high-

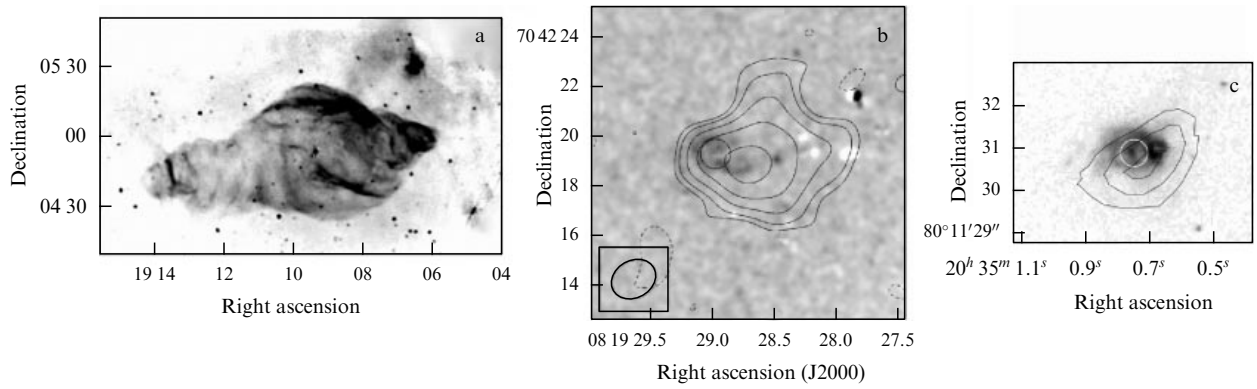

Figure 4. Three nebulae at the same spatial scale. (a) Image of the W 50 nebula [13] with SS 433 in the center, obtained by the VLA radio telescope. (b) Image of the nebula around the Holmberg II ULX, obtained by the HST space telescope in the HeII line with radio isophotes from the VLA radio telescope [24]. (c) The MF 16 nebula in lines Hα+[SII], surrounding the NGC 6946 ULX imaged by HST with the VLA radio isophotes [26]. The CHANDRA observations of X-ray source positions are shown by circles.

resolution images of nebulae in galaxies Holmberg II and NGC 6946, taken in spectral lines by the space telescope. In both cases, (spatially unresolved) radio sources are shifted toward the brightest ring-like structure. According to our data [14, 18], in both cases the part of the nebula coinciding with the radio source moves to the observer. One can imagine that these two nebulae around ULXs are similar to the W 50 nebula surrounding SS 433, and yet with the principal axis close ($i = 10° - 30°$) to the line of sight. We should continue observations to obtain a more reliable sample of nebulae around ULXs.

3. The structure of the funnel in SS 433, X-ray luminosities and spectra of ULXs

We start by briefly describing basic parameters of SS 433 [7] and possible structure of the funnel of the supercritical accretion disk in this system. The persistent and significantly supercritical rate of gas accretion on a black hole ($\sim 10 M_\odot$) is the main feature of SS 433 that makes it distinct from other known X-ray binaries. This leads to the formation of a supercritical accretion disk and relativistic jets. In contrast to jets in other microquasars, which are launched only during outbursts, jets in SS 433 are permanent and 'heavy', i.e., they consist of ordinary gas. The velocity of the jets is virtually constant and reaches 0.26 of the speed of light.

The SS 433 system is observed close to the accretion disk plane, i.e., we cannot view the bottom or internal walls of the funnel. A very bright UV source with $L \sim 10^{40}$ erg s^{-1} and temperature $T = (5-7) \times 10^4$ K [19, 20] is observed, located nearly at the site where relativistic jets appear from beneath a photosphere in the accretion disk wind. The wind mass loss rate equals $\dot{M}_{\rm w} \sim 10^{-5}\, M_\odot$ per year. The optical jets in SS 433 ($\sim 10^{15}$ cm) consist of small dense gas clouds. Both the optical and X-ray jets are strongly collimated ($\sim 1°$). The observed X-ray radiation is formed in X-ray jets being cooled ($\sim 10^{12}$ cm) and the X-ray luminosity is $\sim 10^4$ times smaller than the UV luminosity of the object. However, the 'kinetic luminosity' of the jets is very high: $L_{\rm k} \sim 10^{39}$ erg s^{-1}.

Jets in SS 433 are produced in the supercritical disk funnel. Most likely, the funnel's interior is formed in a thick accretion disk, and the funnel's exterior continues in the dense wind from the disk. Figure 5 schematically shows the funnel. The black square represents the region a few hundred Schwarzschield radii in size, inside which numerical simulations can be performed at present. Two-dimensional hydrodynamical calculations of supercritical accretion disks, accounting for radiation [21, 22], demonstrate that a broad funnel with a total opening angle $\theta_f \approx 40° - 50°$ is formed close to the center. The funnel walls are dynamical. Outside the funnel, convection is important in the inner parts of the disk.

Assuming a luminosity in the funnel to be on the order of the total one in SS 433 [5, 23] and adopting funnel's opening angle obtained from numerical calculations, we can find the 'observed' X-ray luminosity from the funnel in SS 433 to be $L_{\rm X} \sim 10^{41}$ erg s^{-1}, and the expected occurrence rate of such objects ~ 0.1 per Milky Way type galaxy.

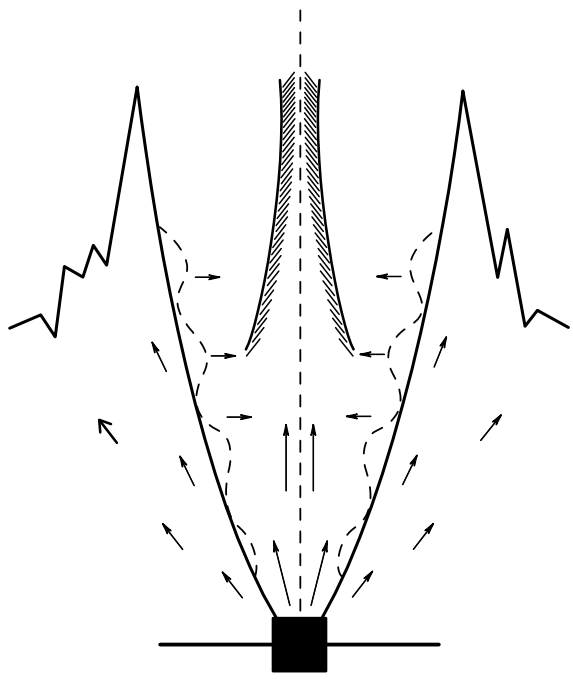

Figure 5. Schematic of the funnel in the supercritical accretion disk in SS 433. The thick curve outlines the funnel photosphere. Shown are the slow wind from the disk (~ 1000 km s^{-1}) and the fast wind inside the funnel that is collimated into a jet at the funnel's outlet.

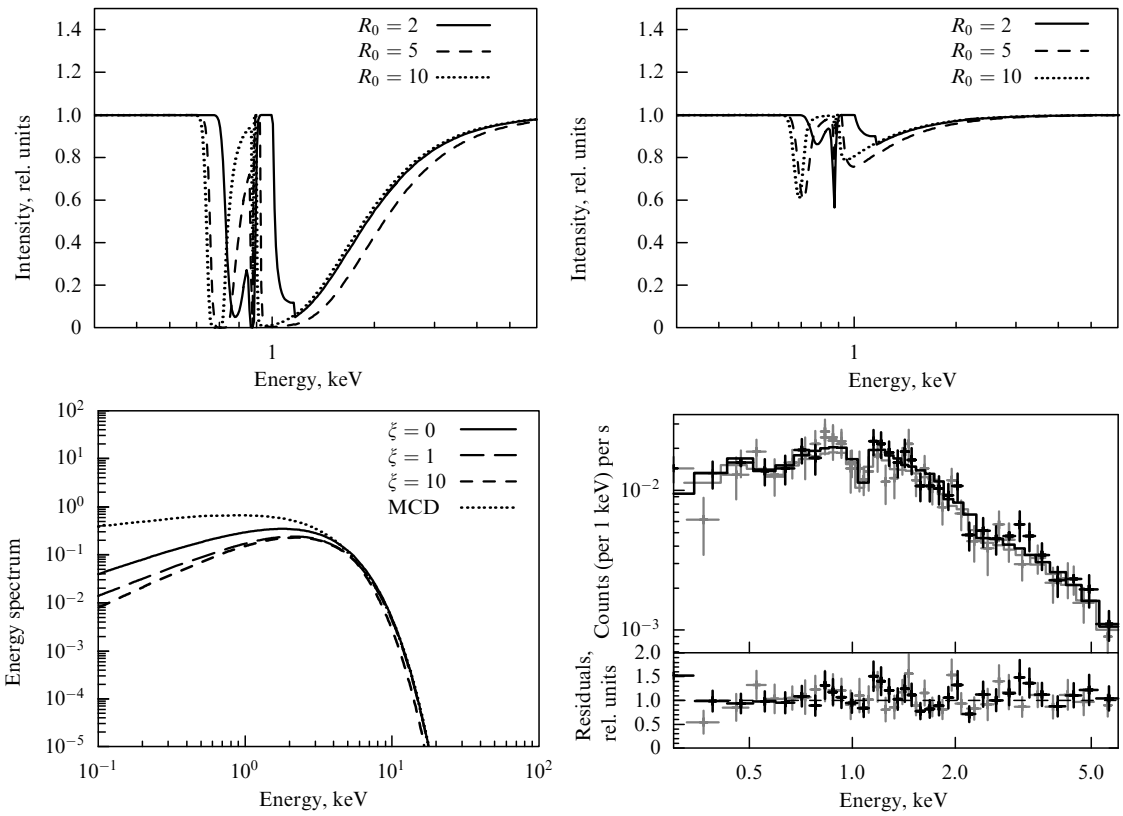

Figure 6. Expected X-ray spectra from the funnel in SS 433. The continuum spectrum (bottom left) is calculated for different radiation-to-gas pressure ratios ξ in the deepest parts of the funnel. Profiles of the OVIII blend of the Lα and Lc transitions for different efficiencies of gas acceleration by jets are shown for optically thick (top left) and optically thin (top right) cases. The gas acceleration starts at $R_0 = 1$ (photosphere of funnel's bottom) and ends at $R_0 = 2, 5, 10$. The bottom right panel shows the spectrum of a ULX in the NGC 4736 galaxy obtained by the XMM-Newton X-ray Observatory.

On the other hand, the critical luminosity of a black hole with mass $10\,M_\odot$ equals $L_{\rm edd} \sim 10^{39}$ erg s^{-1}. At a strongly supercritical accretion rate in SS 433 of $\dot{M}/\dot{M}_{\rm cr} \sim 10^3$, the total disk luminosity exceeds the critical one [3] by $(1 + \ln(\dot{M}/\dot{M}_{\rm cr})) \sim 10$ times. The second factor (relativistic beaming) only mildly increases the observed luminosity, $1/(1-\beta)^{2+\alpha} \sim 2.5$, where $\beta = V_{\rm j}/c = 0.26$ is the jet velocity in SS 433, and α is the X-ray spectral index. The third factor (collimation of radiation by the funnel) is also geometrical, and for the funnel's opening angle $\theta_{\rm f} \approx 40^\circ - 50^\circ$ it amounts to $\Omega_{\rm f}/2\pi \sim 10$. It is seen that the observed (apparent) luminosity from the supercritical disk can amount to $L_{\rm X} \sim 2 \times 10^{41}$ erg s^{-1}, which is consistent with what is observed from ULXs.

To estimate the emerging X-ray spectrum from the funnel, we developed in paper [23] a simplified funnel model (MCF, 'multicolor funnel'). The temperature of the funnel walls was calculated for two limiting cases of the gas temperature in the opaque wind outside the walls: when the gas pressure dominates $[T(r) \propto r^{-1}]$ or when the radiation pressure dominates $[T(r) \propto r^{-1/2}]$. From observations we can infer the temperature of the external funnel photosphere and the funnel's depth (the photospheric level at the bottom is calculated from the known mass loss in the jets). The temperature of the deepest funnel walls available for observations was estimated to fall within the range $1 \times 10^6 - 1.7 \times 10^7$ K.

Figure 6 portrays X-ray spectra of the funnel in the MCF model, calculated for different values of the radiation-to-gas pressure ratio $\xi = aT_0^3/3k_{\rm B}n_0$ in the deepest parts of funnel walls. The temperature of these parts is taken to be $T_0 = 1$ keV. We also plot the X-ray spectrum calculated for the multitemperature disk model MCD ($T_{\rm inn} = 1$ keV), which fits the observed hard spectra of ULX best. Clearly, our MCF model can also explain ULX spectra.

The jet velocity in SS 433 ($0.26c$) and its surprising stability enables one to assume that the line-locking effect [25] is important for acceleration of jets in the funnel. An absorption spectrum with Lc- and Kc-breaks of hydrogen-like and helium-like ions can be emitted by the inner walls of the funnel. The MCF model predicts a very complex absorption spectrum consisting of Kα/Kc and Lα/Lc blends of the most abundant heavy elements.

In Fig. 6, we also plot the calculated profiles of the line OVIII of transitions Lα and Lc. The observed spectrum from ULX in NGC 4736 galaxy as obtained by the XMM-Newton X-ray Observatory is also plotted; different lines show two spectra taken simultaneously by two spectrometers. The residuals obtained after dividing the observed spectrum by a model power-law spectrum with an absorption feature at 1.03 keV are shown. Unfortunately, the spectral resolution of the existing X-ray observatories (and small fluxes from ULXs) do not allow detailed investigation of absorption spectra.

The model for the supercritical accretion disk funnel predicts a very complex X-ray absorption spectrum from a ULX, consisting of blends from transitions Lα/Lc, Kα/Kc of the most abundant elements. Variations of physical parameters of gas in the funnel [velocity, density, temperature, filling factor (jet collimation), etc.] can strongly complicate

the spectrum. Observations of X-ray spectra with high signal-to-noise ratios are required to study such absorption spectra. Nevertheless, the predicted spectral complexity, as well as the dependence of line profiles on the funnel structure, and the gas acceleration and collimation in the funnel, provide remarkable possibilities for direct observational probing of the supercritical accretion disk funnels and relativistic jet formation mechanisms.

We conclude that observations of nebulae surrounding ULXs directly suggest that ULXs are likely to be SS 433 type microquasars and not intermediate mass black holes. Observations of X-ray spectra of ULXs by upcoming new-generation X-ray observatories, which will start operating in a few years, may uncover the intricate spectra of ULXs formed in funnels of supercritical accretion disks around stellar mass black holes.

References

1. Fabbiano G, in *The Hot Universe*: *Proc. of the 188th Symp. of the Intern. Astronomical Union, Kyoto, Japan, August 26–30, 1997* (Eds K Koyama, S Kitamoto, M Itoh) (Dordrecht: Kluwer Acad. Publ., 1998) p. 93
2. Strohmayer T E, Mushotzky R F *Astrophys. J.* **586** L61 (2003)
3. Shakura N I, Sunyaev R A *Astron. Astrophys.* **24** 337 (1973)
4. Grimm H-J, Gilfanov M, Sunyaev R *Astron. Astrophys.* **391** 923 (2002)
5. Fabrika S, Meshcheryakov A, in *Galaxies and their Constituents at the Highest Angular Resolutions*: *IAU Symp. 205*: *Proc. of the 24th General Assembly of the IAU, Manchester, United Kingdom, 15–18 August, 2000* (Eds R T Schilizzi et al.) (San Francisco, Calif.: Astron. Soc. of the Pacific, 2001) p. 268
6. King A R et al. *Astrophys. J. Lett.* **552** L109 (2001)
7. Fabrika S *Astrophys. Space Phys. Rev.* **12** 1 (2004)
8. Colbert E J M, Mushotzky R F *Astrophys. J.* **519** 89 (1999)
9. Miller J M, Fabian A C, Miller M C *Astrophys. J. Lett.* **614** L117 (2004)
10. Madau P, Rees M J *Astrophys. J.* **551** L27 (2001)
11. Margon B *Annu. Rev. Astron. Astrophys.* **22** 507 (1984)
12. Cherepashchuk A *Space Sci. Rev.* **102** 23 (2002)
13. Dubner G M et al. *Astron. J.* **116** 1842 (1998)
14. Fabrika S, Abolmasov P, Sholukhova O (2006) (in preparation)
15. Afanasiev V L, Dodonov S N, Moiseev A V, in *Stellar Dynamics*: *from Classic to Modern*: *Proc. of the Intern. Conf., Saint Petersburg, August 21–27, 2000* (Eds L P Ossipkov, I I Nikiforov) (Saint Petersburg: Saint Petersburg Univ., Sobolev Astron. Institute, 2001) p. 103
16. Abolmasov P, Fabrika S, Sholukhova O (2006) (in preparation)
17. Afanas'ev V L, Moiseev A V *Pis'ma Astron. Zh.* **31** 214 (2005) [*Astron. Lett.* **31** 194 (2005)]
18. Lehmann I et al. *Astron. Astrophys.* **431** 847 (2005)
19. Cherepashchuk A M, Aslanov A A, Kornilov V G *Astron. Zh.* **59** 1157 (1982) [*Sov. Astron.* **26** 697 (1982)]
20. Dolan J F et al. *Astron. Astrophys.* **327** 648 (1997)
21. Eggum G E, Coroniti F V, Katz J I *Astrophys. J. Lett.* **298** L41 (1985)
22. Okuda T et al. *Mon. Not. R. Astron. Soc.* **357** 295 (2005)
23. Fabrika S, Karpov S (2006) (in preparation)
24. Miller N A, Mushotzky R F, Neff S G *Astrophys. J. Lett.* **623** L109 (2005)
25. Shapiro P R, Milgrom M, Rees M J *Astrophys. J. Suppl. Ser.* **60** 393 (1986)
26. van Dyk S D et al. *Astrophys. J. Lett.* **425** L77 (1994)